Eur. Phys. J. B **14**, 363–369 (2000)

THE EUROPEAN PHYSICAL JOURNAL B
EDP Sciences
© Società Italiana di Fisica
Springer-Verlag 2000

Dependence of matrix and substrate on the morphology of nanocermet thin films

S. Hazra[1], A. Gibaud[1,a], P. Laffez[1], and C. Sella[2]

[1] Laboratoire de Physique de l'État Condensé[b], Faculté des Sciences, Université du Maine, 72085 Le Mans Cedex, France
[2] Laboratoire d'Optique des Solides, Université de Paris VI, Case 80, Tour 13–12, 4 place Jussieu, 75252 Paris Cedex 5, France

Received 3 March 1999 and Received in final form 26 July 1999

Abstract. The influence of matrix and substrate on the morphology of three Pt nanocermet thin films has been studied by transmission electron microscopy (TEM), X-ray specular reflectivity and secondary ion mass spectrometry (SIMS). The TEM measurements clearly evidence the presence of metallic nanoparticles inserted in an amorphous insulator matrix. The structure of the thin films in the z-direction, normal to the surface of the films, is then analysed by specular X-ray reflectivity. Using two different models to analyse the data, it is shown that although the size and the mean separation of the particles does not depend much on the nature of the insulator matrix, the substrate and the insulator matrix play a key role at the film-substrate interface. These conclusions are reinforced by the SIMS analysis which shows that the diffusion of metallic particles in the substrate is important in the presence of alumina matrix.

PACS. 68.55.-a Thin film structure and morphology – 61.46.+w Clusters, nanoparticles, and nanocrystalline materials – 61.10.Kw X-ray reflectometry (surfaces, interfaces, films)

1 Introduction

Ceramic-metal (cermet) thin films have been studied for a long time by various techniques because such materials are useful devices for absorbing radiation in the visible and infra-red regions of the solar spectrum [1–4]. The absorption of radiation depends on the concentration and nature of the metallic particles in the cermet films. Technologically, they have been used in solar energy plants, and so far their optical properties have been presented in detail from an experimental point of view but interestingly their morphology is not really understood. The reason for this is related to the fact that such films are composed of granular materials. An appropriate approach to describe their morphology must be a statistical one. It has been shown by transmission electron microscopy (TEM) that the ceramic (insulator) and the metal are imiscible in any proportion. Direct imaging of their morphology especially by TEM is rather demanding due to the preparation of the sample prior to its observation but is nevertheless possible. The information which is obtained is in general the morphology in the plane of the surface. With such a technique (and by resistivity measurements) it was shown that the conductivity of cermets goes from a metallic to a dielectric behaviour when the concentration of the metal is gradually decreased in the cermet. In the metallic regime, the structure is that of an insulator dispersed in the form of isolated particles in a metal continuum. At some critical composition, the insulator particles become interconnected and finally when the metallic concentration is further reduced the structure becomes the reverse of the metallic one. In this case, the metal is dispersed as small grains in the insulator matrix. The metallic grains are very small; the typical size is of the order of a few nm in diameter. This value depends on the nature of the inserted metal. Some attempts have been recently carried out to observe cermets by atomic force microscopy but only the top surface of the film can then be described [5]. Therefore, it was interesting to use alternative techniques to probe the structure of cermets such as X-ray or neutron diffraction techniques. Due to the complexity of the structure, wide angle measurements can give only little structural information about the morphology of these granular films. A very elegant way to derive the structural information of cermet films has been developed by Naudon and Babonneau [6]. In a technique, known as grazing incidence small angle X-ray scattering (GISAXS), the incoming beam impinges on the sample surface at an angle of incidence close to the critical angle for total external reflection and the use of a 2D detector allows the determination of the off-specular scattering at fairly large angles. The anisotropy of the diffuse scattering which is measured on the film is characteristic of the shape and of the separation of the particles. On the other hand, X-ray specular reflectivity and diffuse scattering became extremely powerful techniques to study the structure and interfacial

[a] e-mail: gibaud@aviion.univ-lemans.fr
[b] UPRESA 6087 CNRS

morphology of the thin films. In particular specular X-ray reflectivity has become undisputed in determining the profile of electron density in the direction normal to the surface of a thin film. Widely used in homogeneous thin films or in multilayers, this technique has not yet been much employed to analyse heterogeneous thin films. It is thus challenging to see how far one can go with such a technique in the interpretation of such complex systems. It has been shown recently that reflectivity measurements contain both information about the average thin film itself and about the small grains which compose the cermet [7]. In the method used to analyse the reflectivity [7,8], the average shape of the particles and the average separation between two particles in the z-direction are determined. So far little attention was paid to the interfacial morphology between the cermet and the substrate itself mostly because the previous experiments did not reveal the necessity to take this parameter into account. The use of synchrotron radiation (which allows measurements over two extra decades in intensity) and the study of different matrix and substrates has led us to conclude that the substrate-cermet interfacial morphology could be of crucial importance in the interpretation of the reflectivity curves.

In this paper, we study the influence of the substrate and matrix on the structure of such films. In particular, we use the complementary techniques of X-ray reflectivity, secondary ions mass spectrometry (SIMS) and TEM to study the formation and distribution of Pt nanoparticles within SiO_2 and Al_2O_3 matrix. By depositing Pt nanoparticles within the same Al_2O_3 matrix on silicon and on float glass substrates, we also study how the deposited materials react with the substrate.

2 Experiments

The composite films of Pt-SiO_2 and Pt-Al_2O_3 were made by co-sputtering the amorphous SiO_2 or Al_2O_3 matrix with the metallic Pt clusters on silicon and float glass substrates. The concentration of Pt was monitored by depositing in each case the same number of pellets on the amorphous target of silica or alumina. This number of pellets was fixed to 70. The substrate was rotated during the deposition to ensure the homogeneity of the thin film. Pt-SiO_2 film on silicon substrate and Pt-Al_2O_3 films on silicon and float glass substrates, designated by PSS, PAS and PAG, respectively, which were grown under identical conditions, are presented here.

X-ray measurements were performed both with a laboratory source (Philips diffractometer) and at the synchrotron source (X22A beam line of the NSLS, Brookhaven National Laboratory, New York). The wavelength was either 1.54 Å at the lab or 1.197 Å at the synchrotron source and the full width at half maximum (FWHM) of the direct beam was respectively 0.07° and 0.03°. The major differences in such experiments are the size of the focal spot at the sample position which is much larger on a laboratory experiment than at the synchrotron and the brightness which is orders of magnitude larger at the synchrotron. It is clear that the synchrotron measurements provide much more detail than the ones performed at the laboratory. In particular at high wave-vector values ($q_z > 0.5$ Å^{-1}) normal sources are not powerful enough and the information is lost in the background. X-ray measurements were performed in reflection geometry. In all cases, the X-ray measurements were first made in the specular condition and completed by off-specular scans. Wide angle measurements were also performed which probed the amorphous nature of the insulator and the crystalline state of the metallic inclusions.

To obtain complementary information, we also performed some TEM. These experiments were carried out with a transmission electron microscope working at 200 kV (JEOL 2010) in a high resolution mode. In this case, samples were obtained in a crude way which consisted in scratching the surface of the cermet with a diamond knife. The small part of the film was then deposited on a carbon coated grid of the microscope. Images were also collected from one of the samples in which the TEM sample (in-plane section) was prepared by an ion milling technique. These measurements are presented to give the view of how the granular structure looks like in real space.

SIMS measurements were carried out on the same films. These measurements were made with a CAMECA-IMS-3F device producing a beam of Cs^+ ions of energy 5.5 keV under the incidence of 42°. Under such operating conditions, the depth resolution of the instrument was estimated to be about one nm. During the measurements, the secondary positive M^+ ions and the MCs^+ ions are detected. The intensity of the primary Cs^+ ions' signal is also simultaneously monitored since its value strongly decreases when the beams interact with a light element such as Si [2]. The slope of the SIMS profile at an interface gives some information about the interdiffusion of the two elements on each side of the interface. When the slope is abrupt there is little diffusion and conversely much diffusion in the opposite case.

3 Results and discussion

3.1 TEM

A typical electron diffraction pattern of the PSS film is presented in Figure 1. It is composed of well defined rings which are consistent with the presence of crystallized Pt regions in the film. All the other films also show a similar diffraction pattern. At the scale of the aperture used for the selected area (typically of about a micrometer), the films behave as polycrystalline samples in which the grains display all possible orientations. Direct images of the films are presented in Figures 2a, 2b (PSS film) and 2c, 2d (PAS film) to reveal the nature of the microstructure. It is clear from these figures that two phases coexist. Dark regions were identified as Pt by energy dispersive X-ray (EDX) analysis and appear as rounded particles of nm size. The shape (rounded) and size (~ 30 Å) of the particles are very clear, especially in the TEM image (Fig. 2d)

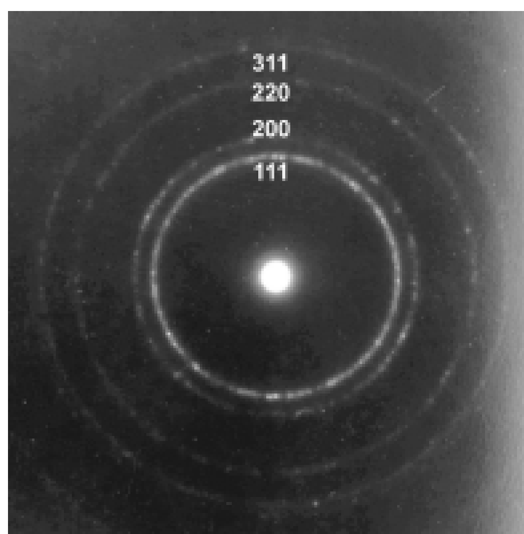

Fig. 1. The electron diffraction pattern of the PSS film. The rings are indexed as Pt.

for which the sample was prepared by an ion milling technique. Fringes at the atomic scale observed within each Pt (dark) region (Figs. 2a–2c) are the indication of crystalline ordering. The Pt clusters are embedded in the alumina matrix which appears in lighter contrast in Figure 2. The alumina matrix does not give rise to any ring in the diffraction pattern of Figure 1 and is therefore amorphous. Tiny differences also appear between the two films. The concentration of Pt in the PAS film appeared to be slightly higher compared to that of the PSS one which is consistent with the different sputtering rate of silica and alumina. The TEM measurements are clearly showing in a direct way that metallic nanoparticles are embedded in the insulator matrix.

3.2 X-ray reflectivity

The specular X-ray reflectivity and the longitudinal off-specular scattering (off-set = 0.12°) of all three films are shown in Figure 3. All the reflectivity curves are similar up to the $q_z \approx 0.20$ Å^{-1}. There is a steep decrease in the reflectivity followed by some small oscillations and an intense hump. After $q_z \approx 0.20$ Å^{-1}, important changes are observed in the reflectivity curves which indicate that all these films present a somewhat different morphology. Two broad humps around 0.25 and 0.40 Å^{-1} are present for both PSS and PAS films having different shapes but are absent in the PAG film. The broad hump around 0.31 Å^{-1} is present for all the films while the broad hump around 0.56 Å^{-1} is only present for the PAS film. The broad hump around 0.12 Å^{-1} is also present in all the off-specular curves. However, its intensity is less by more than 2 orders of magnitude compared to its value in the specular direction. Figures 3a and 3b show the influence of the matrix, while Figures 3b and 3c show that of the substrate.

The steep decrease in the reflectivity observed in the reflectivity curves defines the critical wave-vector (q_c). It is related to the average electron density (ρ) of the film. Experimentally, q_c is found to be 0.047, 0.055 and 0.056 Å^{-1} for PSS, PAS and PAG films, respectively. These values are far less than that of pure platinum (0.083 Å^{-1}) and larger than that of silica (0.032 Å^{-1}) or alumina (0.041 Å^{-1}). The value of q_c or ρ can be used to determine the concentration of Pt in the film. Indeed, one can show that the volume fraction of Pt is given by

$$x = \frac{\rho - \rho_{\text{matrix}}}{\rho_{\text{Pt}} - \rho_{\text{matrix}}} = \frac{q_c^2 - q_{c,\text{ matrix}}^2}{q_{c,\text{ Pt}}^2 - q_{c,\text{ matrix}}^2}\,.$$

The volume fractions of Pt obtained from the above expression are around 0.20, 0.26 and 0.28 for PSS, PAS and PAG films, respectively. Even though these fractions are close, it is clear that the Pt concentration is higher

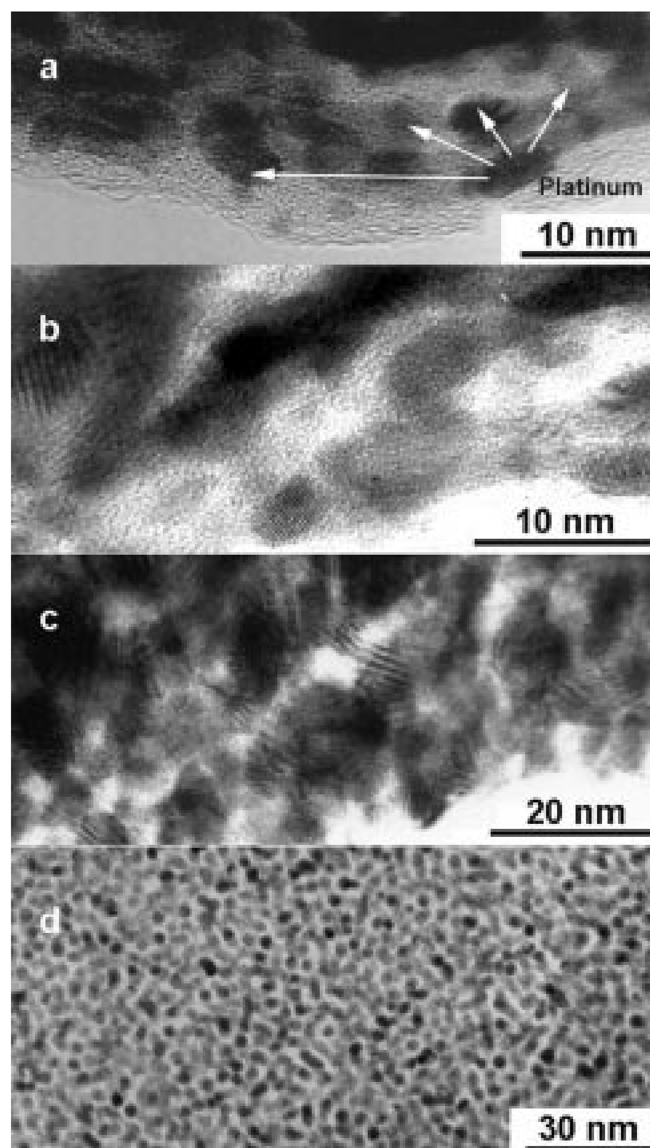

Fig. 2. Transmission electron micrographs of the films illustrating the size and concentration of Pt particles: (a) and (b) for PSS film and (c) and (d) for PAS film.

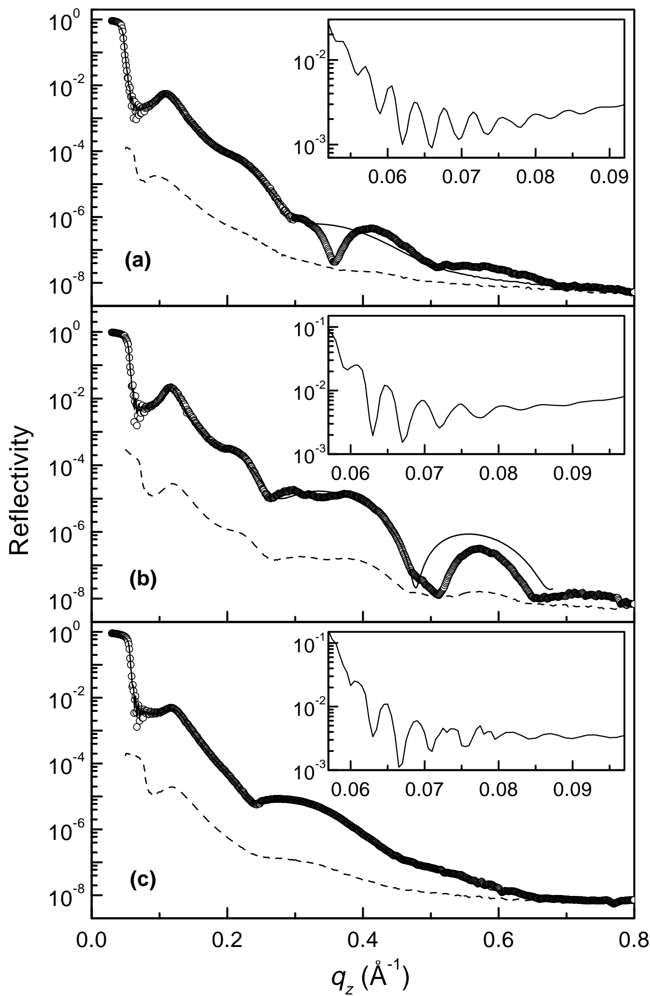

Fig. 3. Reflectivity (o) and the longitudinal diffuse scattering (- - -) for the PSS, PAS and PAG films are shown in panels (a), (b) and (c), respectively. The solid lines drawn through the reflectivity data are the best fit curves obtained from IM. The inset of each panel is the enlarged view of the selected portion of the same reflectivity curve.

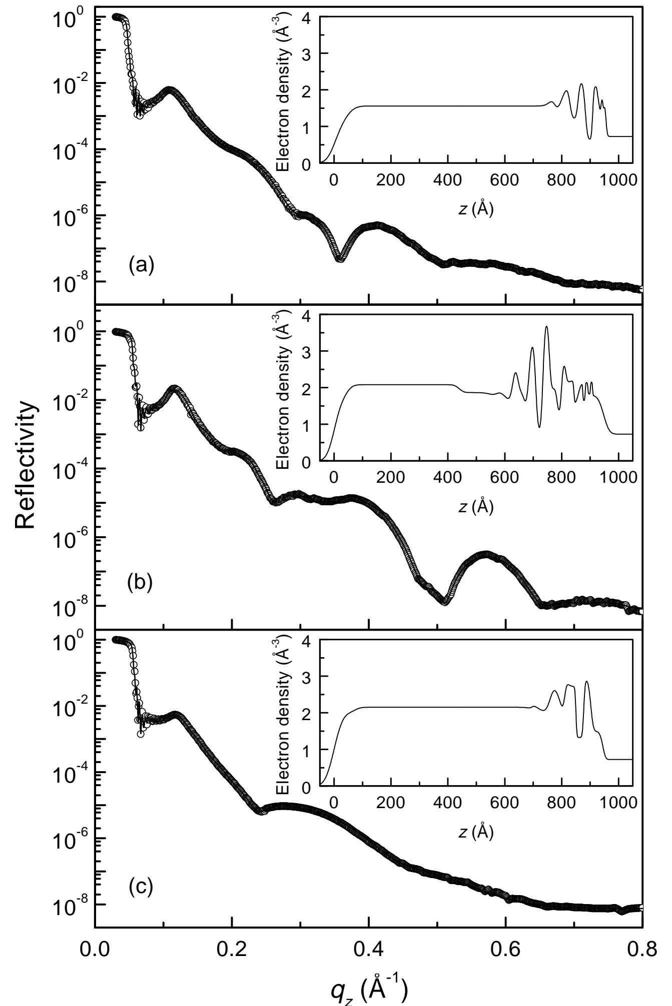

Fig. 4. Best fit reflectivity curves obtained from COM for the PSS, PAS and PAG films are shown in panels (a), (b) and (c), respectively. Corresponding EDP are shown in the inset of each panel.

in the alumina films than in the silica one. This is related to the difference of sputtering rate of silica and alumina. It is known that this rate is higher for silica than for alumina. We must then expect to get a higher Pt concentration in alumina films as we started the co-sputtering with the same amount of Pt pellets in both cases.

The small oscillations observed in the reflectivity curves also shown in the insets of Figure 3 for clarity, known as Kiessig fringes, are related to the total thickness of the films. The location (around 0.12 Å^{-1}) and the intensity of the intense hump are related to the size, concentration and separation of the metallic grains. A crude estimation of the interparticle distance is given by the ratio $2\pi/0.12 = 52.3$ Å.

To obtain more quantitative information, the reflectivity data of all the films were analysed in two ways. The aim is to extract the structure of the films and to test the validity of models to describe the complex structure of heterogeneous thin films.

First, the reflectivity data of all the films are fitted with the matrix technique in which interface roughness is included. The film is divided in slabs of different optical indices. Each slab has its own thickness and electron density or optical index. The slabs are separated by rough interfaces. This model is based on the additivity of the amplitudes reflected by each slab and is thus coherent. We will refer to it as the coherent optical model (COM). The number of different slabs necessary to describe the reflectivity is adjusted according to the complexity of the reflectivity curve. Knowing from the TEM measurements that the cermets are composed of particles and from the reflectivity that the separation of the particles is about 52.3 Å, we have decomposed the film into layers alternatively rich and poor in electron density. The average separation between two rich (or poor) layers was taken as 52 Å, as the starting value and was then allowed to vary together with the electron density in each layer and with the interfacial roughness between the layers. The electron density profile (EDP) obtained from the best fits to the reflectivity data

are shown in the insets of Figure 4 along with the fitted reflectivity curves. For each film, the calculated reflectivity is in fairly good agreement with the experimental data when the EDP presented in the inset is used. The EDP of the three films presents clear similarities which show that the films display, except at the film-substrate interface, a somewhat identical morphology. It is important to notice that the layering does not extend over the whole thickness of the film. This is to our point of view an indication that the ordering of the layers follow a cumulative disordered process as proposed in the second model used to analyse the data. The special ordering which is observed in the PSS and PAS film close to the substrate is responsible for the broad humps near 0.42 and 0.56 Å^{-1}, respectively in the reflectivity curves. In addition, the substrate-film interface is found to be quite sharp for the PSS film and is very broad for the PAS and PAG films. The FWHM of the derivative of the EDP near film-substrate interface are listed in Table 1. The broadening of the interface is the signature that platinum when inserted in the alumina matrix tends to react with the substrate and partly diffuses inside it.

Due to phase loss it is well known that the uniqueness of the solution in a reflectivity analysis can never be guaranteed. In order to check the validity of the EDP, different guess profiles were tested. It was observed that we could fit the reflectivity curves quite closely but with a poorer reliability when, in the EDP used above, the position of the ordered layers was shifted from the bottom to the middle or top of the film. Therefore the COM does not seem to be very sensitive to the position of the enriched Pt layers. The relevant information that we can obtain from the EDP is that, i) the top surface roughness of the films is very big ($\sim$ 40 Å); ii) the films are made of a thick layer of uniform electron density followed by several ordered layers separated by about 53 Å close to the substrate interface; iii) in the immediate vicinity of the substrate this ordering seems to vary with the matrix as well as with the substrate. It is now interesting to compare these results with what can be obtained from the previous model referred to in [7,8].

In order to extract the physical meaning of the above average separation and to know the morphology of the major part of the film, it is assumed that the metal clusters are distributed in the amorphous matrix as observed in TEM. According to that the electron density of the film can be written as [8]

$$\rho(r) = \left[\rho_{\text{matrix}} + \varDelta\rho \sum_i \delta(r - r_i) \otimes S_{\text{Pt}}(r_i)\right] S_{\text{F}}(r)$$

where $\varDelta\rho = \rho_{\text{Pt}} - \rho_{\text{matrix}}$, $S_{\text{Pt}}(r_i)$ is related to the shape and size of the ith cluster at a position r_i and $S_{\text{F}}(r)$ is related to the limited dimension of the film. The total scattered intensity from the film can be calculated in the kinematical approximation as

$$I(q) = \left|\int \rho(r) \mathrm{e}^{-\mathrm{i}q\cdot r} \mathrm{d}V\right|^2.$$

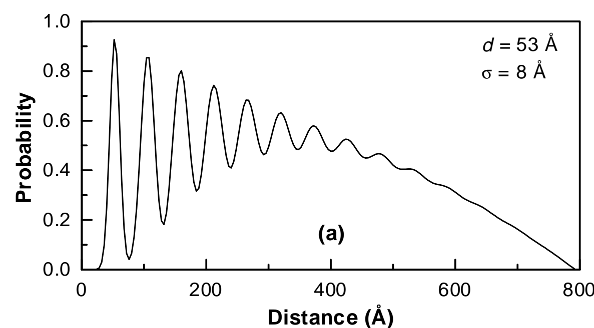

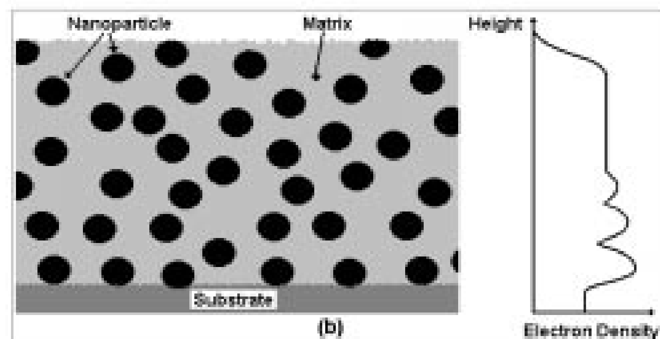

Fig. 5. (a) Typical probability distribution function of Pt particles in the films and (b) schematic diagram of the possible morphology of the nanocermet films along with the EDP.

In this model we assume that the particles can be seen as spherical with an average radius R. This assumption is not unreasonable from the TEM measurements (Fig. 2d). We suppose that they are distributed according to a cumulative disorder process [8,9] along the z-axis. The particles present an average separation d which is the mean distance between two consecutive particles. If the variance associated with the gaussian probability to find this characteristic distance is large ($\sim$ 10% of d) then it is equivalent to saying that the particles will not be stacked with long range order along the z-direction as shown in Figure 5a. If a given particle is in contact with the substrate then only a few particles will be at distances an exact multiple of d from this particle. The given particle will "see" a film of average electron density after a short distance. We then assume that part of the incident beam is reflected by the film interfaces and part of it is scattered by metallic grains having a certain degree of order along the z-axis. Along the direction normal to the surface of the film, one can write the total scattered intensity as the sum of two intensities [7]

$$I(q_z) = I_{\text{matrix}} + I_{\text{Pt}}$$

$$I_{\text{matrix}} = \left|\frac{r_{0,1} + r_{1,2}\mathrm{e}^{\mathrm{i}2q_z D}}{1 + r_{0,1}r_{1,2}\mathrm{e}^{\mathrm{i}2q_z D}}\right|^2$$

$$I_{\text{Pt}} \propto \frac{(\sin q_z R - q_z R \cos q_z R)^2}{(q_z R)^6} \times \frac{1 - \mathrm{e}^{-2q_z^2\sigma_d^2}}{1 - 2\cos(q_z d)\,\mathrm{e}^{-q_z^2\sigma_d^2} + \mathrm{e}^{-2q_z^2\sigma_d^2}}$$

Table 1. Parameters of the nanocermet films obtained from X-ray reflectivity analysis.

Film	Thickness (Å)	Film-substrate Interface (FWHM) (Å)	Pt nanoparticle Volume fraction	Size (Å)	Separation (IM) (Å)	Separation (COM) (Å)
PSS	853	7.3	0.20	29	53	53
PAS	821	37.6	0.26	32	52	54
PAG	867	19.0	0.28	36	50	56

where D is the total film thickness, σ_d is the variance of d. This model is based on the addition of these two intensities and will be referred as the incoherent model (IM). It can be noted that the term I_{Pt} is isotropic in $\mathbf{q}$ space only when the particles in real space are homogeneously distributed in every direction. Any preferential distribution of particles will create anisotropy in $\mathbf{q}$ space. For example if there is any layering of particles along z, then the scattering along that direction will be much more compared to the others. This will not be because of the functional form of the term I_{Pt}, but due to the fact that the proportionality constant, which is related to the number of scatterers responsible for a particular direction, will itself become direction dependent. However, here we are only calculating along the z-direction. Considering another intermediate layer between the film and substrate to take into account the possible interdiffusion, and considering the roughness value, we have calculated I_{matrix}, while I_{Pt} have been calculated by considering size (R), separation (d) and concentration of Pt particle in the film. In this calculation we have neglected the limited dimensional effect of the film on the I_{Pt} calculation. The reflectivity thus calculated for all the films are shown in Figure 3. The calculated and observed data show fairly good agreement up to some q_z values and it gives the average size and separation of the particles in the matrix with their distributions. The size of the particles, interparticle separation and the average thickness of the films are shown in Table 1. From the interparticle separation and from the variance of its distribution, it is possible to get the probability of finding next neighbours in the vicinity of any clusters. The IM provides the Patterson function along the z-direction. Although it does not give any insight on the exact location of the particles because it is basically a statistical description in terms of immediate neighbours but the fact that the intensity at first peak position (~ 0.12 Å^{-1}) in the specular direction is much stronger compared to that in the off-specular direction suggests the formation of layering of particles in the z-direction.

It is interesting to note that the simple layering model (COM) can predict the reflectivity very well and it gives interparticle separation, but can not predict the size and shape of the particles. On the other hand, the IM not only gives the interparticle separation and the size of the particles, but tells us about the formation of layering of particles along the z-direction. So far, the application of these two formalisms brings the structure of the films in a complementary manner and along with TEM gives us some insight about the statistical organization of the Pt clusters in these films. The main information from the TEM is that there are well separated Pt clusters in the plane of these films. From the reflectivity analysis based on two complementary models, one can extract the average size and separation of the particles in the z-direction, the roughness of the top interface and the complex morphology of the film-substrate interface. At this point we would like to stress that the results obtained from the two models do not contradict each other. In both models a characteristic interparticle separation is obtained and a film of average electron density having a rough top surface must be considered. The COM relies on a large number of parameters so it is bound to give better results than the IM. On the other hand the IM gives some extra information since the size of the particles along the z-direction is also determined. Let us now consider the enriched Pt layers. From the goodness of fit it seems that the layering of the particles are close to the substrate. One can argue that this is the most logical expectation since in the making of such films the substrate breaks the symmetry in the z-direction. This type of layering of nearly spherical molecules was recently found in liquid films [12], also the nanoparticles of Ag were found to be well ordered in metallic thin films [13]. As mentioned above the probability distribution function of the particles will be like Figure 5a and correspondingly the film morphology that we would like to propose will be similar to that of Figure 5b. However, the only way to confirm the ordering of particles close to the substrate in the predicted morphology is to perform electron microscopy of a cross-section of the film. It is very difficult to prepare such a cross-section and unfortunately we have not yet been successful in producing it.

3.3 SIMS

The SIMS curves of PSS and PAS films are shown in Figure 6. The measurements were only made on the samples deposited on the silicon substrates since the float glass does not allow evacuation of the electrical charges. More details about the SIMS analysis can be found in [10,11]. In the PAS film, the SIMS profiles of the Cs^+, O^+, Pt^+, $AlCs^+$, $SiCs^+$ show that the interface between the film and the substrate is diffuse. The thickness of the diffuse

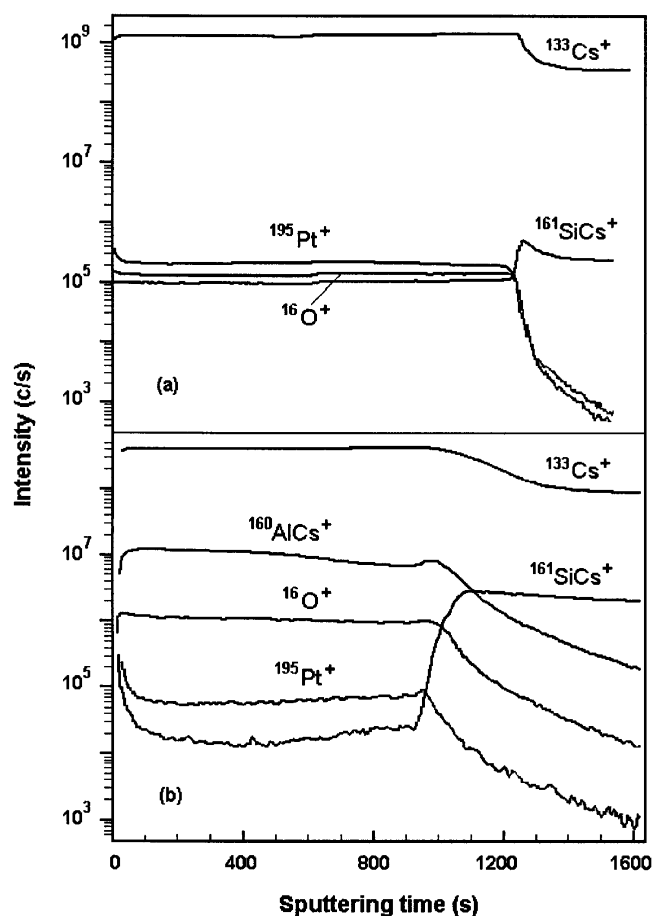

Fig. 6. SIMS curves for PSS and PAS films are shown in panels (a) and (b), respectively.

layer is estimated to a few nm. This seems to evidence that some interdiffusion of the Pt, Al and O elements inside the Si substrate occurs. In the PSS film, the SIMS profiles are much more abrupt at the interface and this is the clear signature that the SiO_2 matrix prevents the interdiffusion. This might be due to the presence of the native SiO_2 layer which is always present at the surface of the bare substrate. These results are in good agreement with the EDP obtained from the reflectivity curves and shown in the inset of Figure 3. Indeed the Si-film interface is quite sharp in the PSS film and diffuse in the PAS film.

4 Conclusion

TEM, X-ray reflectivity and SIMS studies of Pt cermet thin films have been carried out to investigate the influence played by the substrate and the matrix on the morphology of these films. The TEM measurements clearly evidence the presence of nanoparticles embedded in an amorphous silica or alumina matrix. The analysis of the specular X-ray reflectivity shows that the films are made of Pt nanoparticles about 30 Å in size distributed in the amorphous matrix with an average separation of 53 Å. The particles are not stacked with a long range order along the z-direction but exhibit a cumulative disorder process. Due to such a disorder, the film appears as uniform after a few Pt-rich layers which seem from our analysis to be located close to the substrate. The use of synchrotron radiation allows observation of fine features at high wave vector transfers with a reflectivity below 10^{-7}. These features are matrix-dependent. In particular, when the matrix is made of alumina, it is found that Pt diffuses into the substrate (this effect is not prominent with the silica matrix). The interdiffusion is found to be more important for the silicon than for the glass substrate. These results are in very good agreement with the conclusions of the SIMS analysis. Since the above X-ray reflectivity study is restricted to the specular direction, one can only access some structural information in the direction normal to the surface of the films. Apart from the direct view of the films obtained by TEM, we do not have much information about the organization of the films in the direction parallel to their surface. To achieve a complete understanding of their morphology, it would be useful to combine the specular reflectivity measurements to GISAXS experiments to probe at the same time the in and out of plane structure of such films. The direct observation of a cross-section by TEM would also greatly help.

The authors are grateful to the NSLS, Brookhaven National Laboratory, specifically to the members of the X-ray scattering group who let us to use the X22A beamline to measure the reflectivity of the films.

References

1. B. Abeles, P. Shing, M.D. Coutts, Y. Arie, Adv. Phys. **24**, 407 (1975).
2. J.A. Thornton, J.A. Lamb, Thin Solid Films **96**, 175 (1982).
3. G.A. Niklasson, C.G. Grandqvist, J. Appl. Phys. **55**, 3382 (1984).
4. C. Sella, A. Bichri, J.C. Martin, J. Lafait, K. Driss-Khodja, S. Berthier, Physica A **157**, 555 (1989).
5. C. Sella, M. Maaza, B. Pardo, F. Dunsteter, J.C. Martin, M.C. Sainte Catherine, A. Kaba, Surf. Coat. Tech. **97**, 603 (1997).
6. A. Naudon, D. Babonneau, Z. Metallkd **88**, 596 (1997).
7. M. Maaza, A. Gibaud, C. Sella, B. Pardo, F. Dunsteter, J. Corno, F. Bridou, G. Vignaud, A. Désert, A. Menelle, Eur. Phys. J. B **7**, 339 (1999).
8. A. Gibaud, C. Sella, M. Maaza, L. Sung, J.A. Dura, S.K. Satija, Thin Solid Films **340**, 153 (1999).
9. B.K. Vainshtein, in *Diffraction of X-rays by Chain Molecules* (Elsevier, Amsterdam-London-New York, 1966).
10. C. Sella, M. Miloche, O. Nemraoui, in *Proc. of the 10th International conference on SIMS, SIMS-X* (John Wiley, 1997), pp. 411–414.
11. O. Nemraoui, M. Miloche, M. Kaabouchi, C. Sella, J. Phys. IV France **6**, C7–31 (1996).
12. C.-J. Yu, A.G. Richter, A. Datta, M.K. Durbin. P. Dutta, Phys. Rev. Lett. **82**, 2326 (1999).
13. S. Kundu, S. Hazra, S. Banerjee, M.K. Sanyal, S.K. Mandal, S. Chaudhuri, A.K. Pal, J. Phys. D **31**, L73 (1998).